Nonmetal ordering in $TiC_{1-x}N_x$: Ground-state structure and the effects of finite temperature

Brian Kolb and Gus L. W. Hart

Northern Arizona University, Flagstaff, Arizona 86011, USA

The $TiC_{1-x}N_x$ system has long been prized in industry because of its desirable thermodynamic and hardness characteristics. Previous studies have not produced comprehensive results describing the ordering tendencies of $TiC_{1-x}N_x$ at any temperature. We apply the mixed-basis cluster expansion and Monte Carlo methods to the problem and find a fascinating array of ground-state structures occurring at precise nitrogen-concentration intervals of $\Delta x = 1/16$ and related to each other by simple (201) quasisuperlattice motifs. Thermodynamic Monte Carlo results indicate that the critical ordering temperatures at all concentrations are well below room temperature. Short-range ordering develops at $T \approx 800$ K and exhibits the characteristic motifs of the predicted ground-state structures. Bulk modulus optimization is not feasible since this quantity shows little sensitivity to atomic configuration.

I. INTRODUCTION

The computational power of first-principles-based model Hamiltonians is revolutionizing our understanding of the ($T=0$) ground states of many binary alloys. A recent Physical Review Letter[1] discussed the discovery of a rich sequence of ground states hitherto unknown in the FeCo system. Intriguingly, these ground states appear at regular Fe concentration intervals of $\Delta x = 1/16$ (on $1/2 \leq x \leq 1$) and exhibit an interesting ordering motif. The authors of Ref. 1 speculate that the existence of many ground states is more common in intermetallic binary systems than previously thought. This viewpoint is corroborated by the recent discoveries of complex sequences of ground-state structures in the MoTa,[2] CuAu,[3] and NiPt (Ref. 3) systems using a similar computational approach.

We report here a similar discovery made in the $TiC_{1-x}N_x$ system. This alloy is important industrially because of its desirable properties (high melting point, corrosion and wear resistance, and high hardness) and is widely used as a coating for high-impact machine parts such as drill bits and other cutting tools. Using the mixed-basis cluster expansion (MBCE) technique[4–8] we have uncovered a rich collection of ground states occurring at nitrogen-concentration intervals of precisely $\Delta x = 1/16$, in the nitrogen concentration range $0 \leq x \leq 1/2$. Further, the atomic configuration of these ground-state structures follows a systematic progression; each structure can be thought of as a (201) quasisuperlattice[44] possessing eight-plane periodicity. Previous works[9,10] have overlooked this behavior because they focused on only a few select structures and not on an exhaustive, direct enumeration approach as applied here.

Few experiments have been performed on $TiC_{1-x}N_x$ to detect long- or short-range order on the nonmetal sublattice, either with or without nonmetal vacancies. X-ray[11] and neutron[12] diffraction experiments have produced results rejecting particular atomic configurations, but have not ruled out the possibility of other ordering schemes or the existence of short-range order. Ordering of structural vacancies is known to exist in both substoichiometric TiC (Refs. 11 and

13) and TiN.[14] We present in this paper the predicted ($T=0$) ground-state structures as well as the results of thermodynamic Monte Carlo simulations and their implications toward the presence of short-range ordering in the stoichiometric $TiC_{1-x}N_x$ system.

II. APPROACH

The cluster expansion is a generalized Ising model, which produces a model Hamiltonian capable of rapid calculation of target material properties as a function of atomic configuration. A brief description of the method and its application herein is given below. A more detailed discussion may be found in Refs. 4–8.

It can be shown[15] that, for a binary alloy, any property Z that is a function of atomic configuration σ may be expressed as

$$Z(\sigma) = J_0 + \sum_i J_i \hat{S}_i + \sum_{i,j} J_{ij} \hat{S}_i \hat{S}_j + \sum_{i,j,k} J_{ijk} \hat{S}_i \hat{S}_j \hat{S}_k + \dots \quad (1)$$

where $\hat{S}_i = \pm 1$ describes the occupation at site i and the J's are expansion coefficients.

Equation (1) taken over all lattice-site interactions produces an exact representation of the property $Z(\sigma)$, but its primary usefulness is as an approximation scheme. A small number of terms chosen judiciously[16,17] from Eq. (1) give an accurate approximation to the exact value of Z. The truncated form of Eq. (1) can be evaluated very quickly and provides a rapid means of calculating physical quantities for any atomic configuration. The expansion coefficients must be chosen such that the model both reproduces known data *and* provides accurate predictions. This is accomplished by furnishing a sizable input set of first-principles data and testing the predictive accuracy of the model.

In the present study, first-principles calculations were performed using the Vienna *ab-initio* simulation package (VASP) pseudopotential code operating within the local density approximation.[18,19] These calculations were performed using an equivalent k-point division scheme[20] to effect systematic
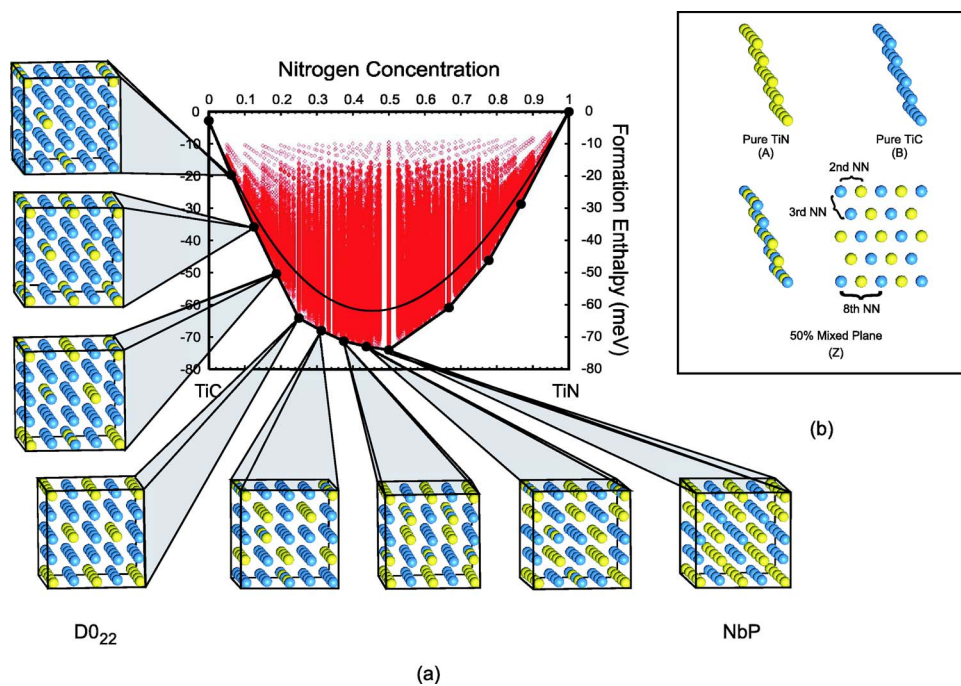
FIG. 1. (Color online) (a) Formation enthalpy calculations for all structures up to 20 C/N atoms/unit cell. Breaking point structures are indicated by the dark circles along the convex hull. Note the minimum energy at $x=1/2$. Also pictured is the formation enthalpy of the random alloy, which may be calculated via the cluster expansion since, for a random configuration, Eq. (1) reduces to $E_{rand}=\Sigma_i J_i(2x-1)^n$ where n is the order of the interaction (i.e., pair, triplet, etc.) (Ti atoms not shown). (b) The three types of C/N (201) planes found in $TiC_{1-x}N_x$ ground states. Also shown are several important nearest-neighbor (NN) geometries within the (201) planes.

cancellation of discretization errors. Full atomic relaxations were performed using a conjugate gradient algorithm. Total energies were converged to within 0.1 meV/atom. All calculations treated titanium $3p$ semicore electrons in the valence. Because of the large antisite defect energies in this system, it is extremely unlikely for a titanium atom to be found on the C/N sublattice, meaning that titanium does not represent a configurational degree of freedom.

Sixty-one relatively low-energy input structures, each with unit cells of up to 8 C/N atoms (16 atoms total) were calculated as input to the cluster expansion. Predictions were calculated for *all* atomic configurations with unit cells of up to 20 C/N atoms ($\approx 3 \times 10^6$ structures). The predictive accuracy of the model was tested with a leave-many-out cross validation approach[5,21–23] and by direct calculation of select predictions. The average prediction error of the model is 2.7 meV/atom. Monte Carlo simulations were used to determine critical ordering temperatures ($16 \times 16 \times 16$ atom cell with 1000 spin flips/site/annealing step) and short-range order ($20 \times 20 \times 20$ atom cell with 1500 flips/site/step). Crystal orbital Hamilton population[24] (COHP) calculations were performed using the tight-binding linear muffin-tin orbital (TB-LMTO) code version 47 operating under the atomic-sphere approximation.[25,26]

III. RESULTS AND DISCUSSION

A. Ground-state determination

Formation enthalpies for all $TiC_{1-x}N_x$ structures with 20 C/N sites or less calculated via the MBCE method are shown in Fig. 1(a). These results are consistent with previous findings, which showed complete miscibility of the TiC/TiN systems.[9] However, our results indicate an energy minimum at $x=1/2$ in contrast with Refs. 9 and 10, which place the minimum at $x=1/4$. Test calculations performed with parameters similar to those used in these references produced results consistent with those presented here. In addition, calculations using more accurate projector augmented wave (PAW) potentials[27,28] were performed and, again, results were consistent with those presented here. Further tests indicate that the discrepancies between our results and those in Refs. 9 and 10 are largely a result of their failure to consider Ti $3p$ electrons in the valence and by differences in pseudopotentials and cutoff energies. As a secondary check to our calculations, a cluster expansion was constructed for lattice constants. The results showed nearly Vegard-like behavior over the entire range of concentration (as measured experimentally) with all values lying $\lesssim 1.3\%$ below experimental values,[29,30] a feature typical of density functional theory calculations.

The first thing to note about Fig. 1 is that all the calculated formation energies are negative. The reason for this can be understood by investigating band-filling via COHP (Ref. 24) calculations for the TiC and TiN end points. These calculations show that the TiC Fermi level falls in a slightly bonding region. Any extra electrons added to the system would populate these states and improve Ti-C bonding. The situation is reversed in TiN, where antibonding states are populated by electrons near the Fermi level. Removal of electrons from the TiN system would enhance the Ti-N bonding. $TiC_{1-x}N_x$ is stable because electrons can vacate some of the TiN antibonding states and populate the TiC bonding states leading to an overall improvement in bonding. This analysis parallels the band-filling arguments discussed in previous works.[31–33]

The $TiC_{1-x}N_x$ convex hull exhibits several fascinating characteristics. The existence of numerous breaking points—thermodynamically stable structures represented by the dark circles in Fig. 1(a)—is a feature often absent in intermetallic binary alloys. Many binaries have only a handful of breaking points, in sharp contrast to the 13 found in the $TiC_{1-x}N_x$

TABLE I. Observed stacking sequences of (201) planes in TiC$_{1-x}$N$_x$ ground states. Here, A is a pure nitrogen plane, B is a pure carbon plane, and Z is a plane consisting of 50% nitrogen and 50% carbon. In each case there are 8 C/N planes comprising the stacking sequence.

Concentration	(201)-layering	Archetype
1/16	$Z\ B\ B\ B\ B\ B\ B\ B$	
2/16	$Z\ B\ B\ B\ Z\ B\ B\ B$	
3/16	$Z\ B\ B\ B\ A\ B\ B\ B$	
4/16	$A\ B\ B\ B\ A\ B\ B\ B$	$D0_{22}$
5/16	$A\ Z\ B\ B\ A\ B\ B\ B$	
6/16	$A\ Z\ B\ B\ A\ Z\ B$	
7/16	$A\ A\ B\ B\ A\ Z\ B\ B$	
8/16	$A\ A\ B\ B\ A\ A\ B\ B$	NbP

system. Even more intriguing is the regular spacing of these breaking points. In the concentration range $0 \leqslant x \leqslant 1/2$, the breaking points occur at concentration intervals of precisely $\Delta x = 1/16$, a feature similar to the one observed in the FeCo system[1] (as mentioned in the Introduction). Further, although the breaking-point structures need not look alike, the TiCN ground states, up to $x = 1/2$, certainly do show a systematic progression. Each ground state in this concentration range can be described as a (201) quasisuperlattice with a stacking period of 8 C/N planes. All such (201) planes are comprised of either pure nitrogen, pure carbon, or a 50% mixture of each, hereafter denoted A, B, and Z, respectively [see Fig. 1(b)].

Table I gives the observed (201)-plane stacking sequences for all ground-state structures up to $x = 1/2$. These sequences may be understood by thinking in terms of adding nitrogen atoms to a 16 atom unit cell (easily visualized as eight layers of two atoms each). The first nitrogen added to the cell forms 50% planes separated by seven pure carbon planes (ZB_7). Addition of a second nitrogen again forms 50% planes, with the position bisecting the distance between the previous 50% planes (ZB_3ZB_3). A third nitrogen is added to one of the 50% planes, converting it to a plane of pure nitrogen (ZB_3AB_3) and a fourth adds to the remaining 50% plane, forming another pure nitrogen plane. At this point, the system is in the $D0_{22}$ structure, an AB_3 superlattice.

The progression from $D0_{22}$ to NbP (an A_2B_2 superlattice) follows a similar pathway. The first nitrogen is added to $D0_{22}$ to form a 50% nitrogen plane adjacent to a pure nitrogen plane and separated from the next 50% nitrogen plane by seven interstitial planes (AZB_2AB_3). The next nitrogen again adds adjacent to a pure nitrogen plane (AZB_2AZB_2). The next two successive nitrogens fill in these two 50% planes in turn, forming NbP.

The breaking-point structure at $x = 2/3$ is a (110) qausisuperlattice with a BZ_2 stacking sequence (Fig. 2). The remaining breaking points do not exhibit such simple ordering motifs. The breaking point at $x = 7/9$ can best be described as a (110) quasisuperlattice with a pure plane followed by two planes at a 2/3 concentration. The final breaking- point at $x = 13/15$ is a true (12,12,1) superlattice with a BA_7BA_6
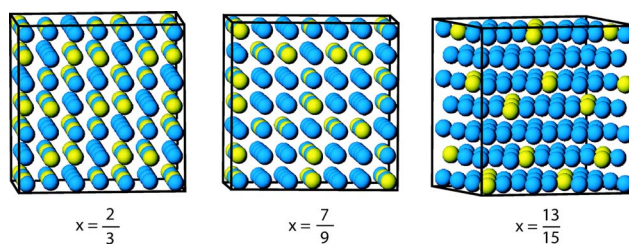

FIG. 2. (Color online) The three breaking point structures on $x > 1/2$.

stacking sequence. These three breaking points are shown in Fig. 2.

The observed arrangement in the 50% (201) planes [see Fig. 1(b)] for structures with $x \leqslant 1/2$ can be understood by looking at the cluster expansion. Figure 3 shows the coefficients corresponding to the many-body figures used in this expansion. The only pair figure energetically favoring a like-atom interaction is the eighth nearest-neighbor pair. Although the third nearest-neighbor pair interactions favor unlike atoms, the small magnitude of this term means that the energetic costs of a like-atom third nearest neighbor arrangement are small compared to like atoms at other distances. When (201) planes are arranged as shown in Fig. 1(b), all second nearest-neighbor pairs are of unlike atoms. This is a favorable arrangement as indicated by the positive value of the P_2 expansion coefficient. Considering both third and seventh nearest-neighbor interactions, half are of like atoms and half are of unlike atoms so the P_3 and P_7 interactions within these planes do not contribute to the total energy. All eighth nearest-neighbor pairs are of like atoms. No other pair interaction less than eighth nearest neighbor (the longest pair term used in the expansion) exist within (201) planes. Thus, forming 50% planes as illustrated in Fig. 1(b) lowers the total energy and such planes are preferentially formed.

This description for the ordering of TiC$_{1-x}$N$_x$ in terms of pair interactions does not account for why the ground-state line for $x > 1/2$ looks different than that for $x \leqslant 1/2$. Clearly, pair interactions alone cannot account for this since their effects are symmetric about $x = 1/2$. The large positive J_1
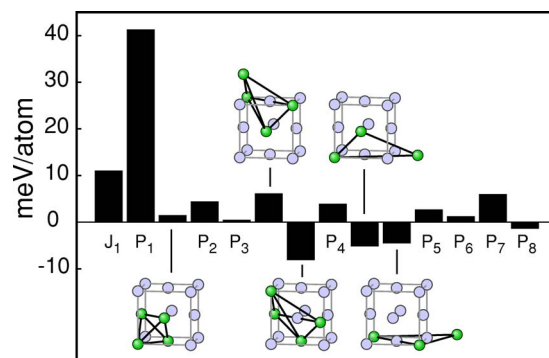

FIG. 3. (Color online) Coefficients corresponding to the many-body interactions (figures) used in the cluster expansion. Here, P_n refers to the nth pair. Also shown are the geometries of the higher order interactions used (i.e., three-body and four-body) for the C/N fcc sublattice. The figures are placed in order of increasing longest-vertex distance (not to scale).

term tends to raise the energy of the TiN-rich structures off of the convex-hull leaving fewer breaking points on that side. To understand why the TiN-rich breaking points exhibit different motifs than the TiC-rich ones, we must look at higher-order terms. Since the effect of three-body terms is antisymmetric about $x=1/2$, such terms will tend to reorder the structures on the right-hand side. Three-body terms that stabilize structures where $x<1/2$ will have the opposite effect on structures where $x>1/2$. Thus, the chemical effects governing structural stability on the right half of Fig. 1 are not necessarily the same as those on the left half.

Of the breaking point structures, the two true (201) superlattices, $D0_{22}$ and NbP (AB_3 and A_2B_2, respectively), are particularly stable. Most of the breaking points evident in Fig. 1(a) are relatively shallow but those at $x=1/4$ and $x=1/2$ are especially deep. In addition, the energy differences between these structures and those immediately above them in energy are much larger than the differences for the other breaking points. These two observations indicate special stability in these breaking points. This stability stems largely from the fact that *all* eighth nearest-neighbor pairs in these structures are of like atoms. It is interesting to note that, for both $x=1/4$ and $x=1/2$, the difference between the ground-state structures and their immediate, higher-energy neighbors (at the same concentration) are simple (001) stacking faults, which break the superlattice symmetry by introducing impure (201) planes.

B. The physical origins of the (201) stacking motif

There are two major players in determining the ordering behavior of any alloy: strain energy and chemical energy. Strain energy typically arises from lattice mismatch between the constituent species, and is generally different for distortions in different crystallographic directions. In view of this, we may ask what role strain plays in determining the preferred superlattice direction for this system. The small lattice mismatch between TiC and TiN ($\approx 2\%$) hints that strain energies are likely to be small. Full strain calculations (see Fig. 4) for the TiCN system confirm that strain energies are, indeed, small. Figure 4 illustrates the directional dependence of the constituent strain energy. The largest strain energies for this system arise from distortions in the (111) direction, particularly at higher nitrogen concentration. Strain energies associated with distortions in directions other than (111) are not only considerably smaller, but are all comparable in magnitude, indicating that strain effects are relatively independent of superlattice direction.

Since, with the possible exception of the [111] direction, strain plays essentially no role in determining ordering behavior for this system, we look to chemical effects to find why (201) superlattices are preferred. Although we have discussed the ground-state structures in terms of C-N interactions, the stability of particular C/N atomic configurations has more to do with producing a favorable chemical environment around the interstitial Ti atoms. The bonding in crystalline $TiC_{1-x}N_x$ is dominated by the Ti-C and Ti-N first-nearest-neighbor bonds. Other bonds, most notably Ti-Ti second-nearest-neighbor bonds, play only a minor role in
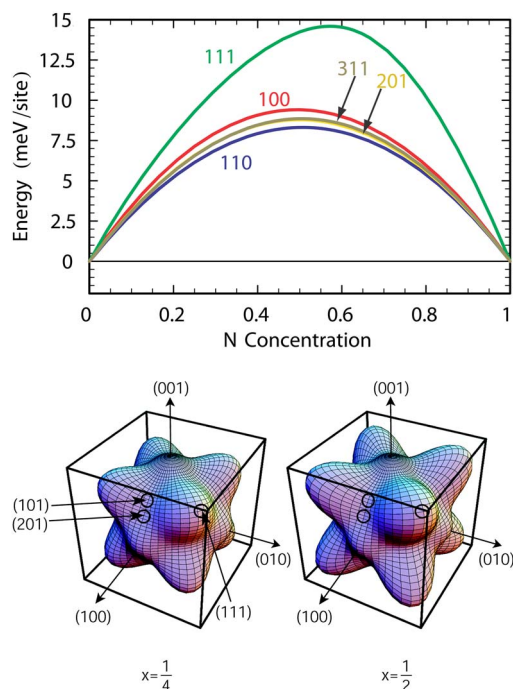

FIG. 4. (Color online) (Top) Constituent strain energies as a function of concentration for several important crystallographic directions. (Bottom) Plot illustrating the directional dependence of strain energy for both the $x=1/4$ and $x=1/2$ concentrations. The arrows and black circles indicate some important crystallographic directions. The radius from the center of the cube to the surface at a given point gives the relative magnitude of the strain energy in that direction. In all cases, the strain energy is less than 15 meV/atom.

determining the alloy stability. As already mentioned, band-filling arguments place the optimum bonding interaction at a valence electron count (VEC) intermediate between that of TiC (8.0) and TiN (9.0). The preference toward forming (201) superlattices arises from the fact that this arrangement is a very efficient way to obtain optimum VECs around the titanium atoms. For example, in the lowest-energy structure (NbP) every titanium atom has a first-nearest-neighbor coordination shell containing three carbon and three nitrogen sites for a VEC of 8.5. Similarly sized superlattices in the (001) and (011) directions contain several symmetry-inequivalent titanium atoms which have much poorer VECs. Superlattices in the (111) direction are unlikely because of the increased strain associated with that direction. This result that chemical energy is minimized for a VEC of ≈ 8.5 is not unlike recent reports that transition metal alloys adopting the rock-salt structure have optimum hardness for a VEC of 8.4 electrons/cell.[34] It should be pointed out that this sequence of structures and the (201) ordering motif can be interpreted in terms of special-point concentration waves.[35]

C. $TiC_{1-x}N_x$ at finite temperature

Since our model Hamiltonian can be quickly evaluated for any atomic configuration, it may be used in conjunction with Monte Carlo simulations to model the effects of finite temperature on the ordering tendencies of $TiC_{1-x}N_x$. These cal-

culations show that the critical ordering temperatures are well below room temperature at all concentrations. Such low transition temperatures are a direct result of the small ordering enthalpy [the difference between the random alloy enthalpy and that of the ground-state configuration at a given temperature, see Fig. 1(a)]. At finite temperatures, the entropic contribution to the free energy has little competition from chemical interactions and a moderate increase in entropy improves the thermodynamic stability of the solid solution. Diffusion is likely to be extremely limited at temperatures sufficiently low to allow the chemical energy contribution to dominate the free energy, making ordered-phase formation unlikely in TiC$_{1-x}$N$_x$ solid solutions.

The sign of the ordering enthalpy, however, indicates that ordering is chemically favorable and suggests the possibility of short-range ordering, an assertion that is corroborated by Monte Carlo simulations, which show short-range order at temperatures $\lesssim 800$ K. The nature of this ordering can be ascertained by extracting from Monte Carlo simulations performed above the order-disorder transition temperatures the Fourier-transformed Warren–Cowley[36–38] short-range order parameters, given by

$$\alpha(\mathbf{k},x) = \sum_{\mathbf{k}} \frac{\sum_{i,j} \hat{S}_i \hat{S}_j - (2x-1)^2}{1 - (2x-1)^2} e^{i\mathbf{k}\cdot\mathbf{R}}, \quad (2)$$

where the inner sum is taken over all pair figures up to some practical limit.[39]

The significance of α lies in its ability to enumerate pair correlations of a particular atomic configuration and, hence, the degree of ordering. The value of α will only be nonzero at reciprocal-space points corresponding to nonrandom pair figures. Thus, a reciprocal-space plot of $\alpha(\vec{k})$ exhibits peaks at only those points corresponding to the periodicity of the structure. The degree of ordering is correlated to the peak width, with peaks narrowing as pair correlations become more long ranged.

In the case of TiC$_{1-x}$N$_x$, the fully ordered structures at both $x=1/4$ and $x=1/2$ give peaks at $[0,1,1/2]$, $[1,0,1/2]$, $[1,2,1/2]$, and $[2,1,1/2]$, corresponding to the (201) super-lattice ground-states. Figure 5 shows plots of $\alpha(\vec{k},x)$ in (002) slices through the reciprocal lattice at several temperatures for the $x=1/4$ and $x=1/2$ concentrations. As is evident by the peaks at the aforementioned positions, at temperatures of $\lesssim 800$ K the system shows ordering with motifs similar to those of respective ground-state structures. The broadness of the peaks indicates that this ordering is prevalent over relatively short distance scales, but the peaks are clearly narrowing as the temperature is decreased, indicating that ordering patterns are becoming more long ranged. The ordering becomes significant at temperatures nearing room temperature.

For both the $D0_{22}$ and NbP structures (the breaking points at $x=1/4$ and $x=1/2$, respectively), internal and external relaxations are minimal. In fact, the c/a ratio in both cases is $\lesssim 0.1\%$ different from the ideal value. We, therefore, expect diffraction spectra to show minimal diffuse scattering signal due to displacements off the ideal atomic sites. At both
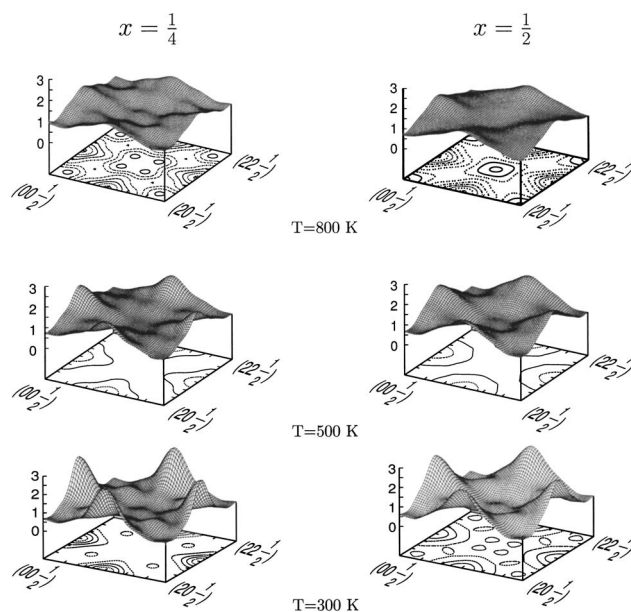

FIG. 5. Plots of α showing short–range ordering as a function of concentration and temperature. The fully ordered structures at both concentrations would have peaks at $\left(01\frac{1}{2}\right)$, $\left(10\frac{1}{2}\right)$, $\left(12\frac{1}{2}\right)$, and $\left(21\frac{1}{2}\right)$.

$x=1/4$ and $x=1/2$ the spectra should be dominated by the signal due to atomic configuration.

D. Bulk modulus

The hardness of a material is a complex quantity that is intimately connected with the formation and movement of dislocations through the lattice. There are many measures of hardness and while bulk modulus alone does not give a definitive measure of material hardness it does serve as a guidepost to the structural stability and is readily calculated within the framework of *ab initio* methods. A plot of bulk modulus versus nitrogen concentration is shown in Fig. 6. It is apparent from the small spread of bulk moduli at each concentration that this quantity expresses a lesser sensitivity to atomic configuration than does the formation enthalpy. The largest spread of values observed at any concentration is less than 10 GPa. The random-alloy bulk modulus extends in a roughly linear fashion from its minimum at TiC (276 GPa) to
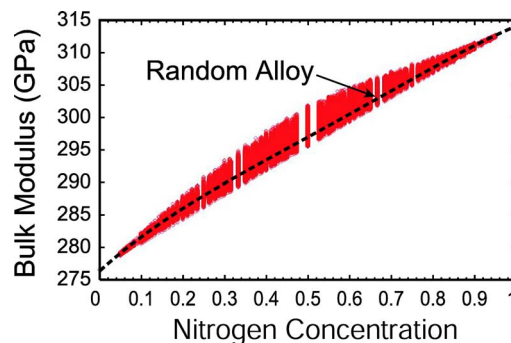

FIG. 6. (Color online) Bulk modulus predictions for all structures up to 20 C/N atoms/unit cell. Also indicated is the bulk modulus of the random alloy (dashed line).

its maximum value (314 GPa) at TiN in good agreement with experiment and previous calculations.[9,40–43] Because of the comparatively small spread in bulk moduli, any degree of short-range ordering is unlikely to cause a significant deviation from the bulk modulus of the random alloy.

IV. CONCLUSION

We have used the mixed-basis cluster expansion method to determine the structure and energetics of the $TiC_{1-x}N_x$ system and have found the minimum energy to be that of the *NbP* structure. Further, we have discovered a rich ground-state line, characterized by (201) quasisuperlattice breaking points occurring at regular concentration intervals of $\Delta x = 1/16$. These structures show a systematic progression from one to the next as the nitrogen concentration is increased through the range $0 \leq x \leq 1/2$. The stacking sequences found in these breaking points can be described in terms of the cluster expansion interaction figures, specifically the preference of forming like-atom eighth nearest neighbor configurations. These results bear a striking, conceptual resemblance to those recently found in the FeCo system.[1] Because of increased filling of Ti-C bonding states and reduced filling of Ti-N antibonding states, Ti-C and Ti-N bonds are strongest when the average valence electron count around each titanium is ≈ 8.5. This feature of the TiCN system is responsible for its preferential formation of (201) superlattices (or quasisuperlattices).

Monte Carlo calculations indicate that the critical ordering temperatures are below room temperature for all concentrations. Since diffusion is limited at such low temperatures, it is extremely unlikely that the system will exhibit long-range ordering. The negative ordering enthalpy suggests that short-range order is favorable, and Monte Carlo simulations confirm that short-range order at finite temperature does indeed reflect the characteristic long-range ordering of the predicted ground-state structures.

Bulk modulus calculations were consistent with experimental bulk moduli and showed only mild sensitivity to atomic configuration. The minimal reaction of bulk moduli to changing atomic configuration means that any degree of short-range order will not cause a significant deviation of the bulk modulus from that of the random alloy, which runs almost linearly from TiC up to TiN. The random alloy bulk modulus curve exhibits some bowing, especially at low-nitrogen concentrations. This bowing is slight, however, and there exists no intermediate concentration at which the bulk modulus exceeds that of TiN.

[1] R. Drautz, A. Diaz-Ortiz, M. Fähnle, and H. Dosch, Phys. Rev. Lett. **93**, 067202 (2004).

[2] V. Blum and A. Zunger, Phys. Rev. B **69**, 020103(R) (2004).

[3] M. Sanati, L. G. Wang, and A. Zunger, Phys. Rev. Lett. **90**, 045502 (2003).

[4] D. B. Laks, L. G. Ferreira, S. Froyen, and A. Zunger, Phys. Rev. B **46**, 12587 (1992).

[5] V. Blum and A. Zunger, Phys. Rev. B **70**, 155108 (2004).

[6] A. Zunger, L. G. Wang, G. L. W. Hart, and M. Sanati, Modell. Simul. Mater. Sci. Eng. **10**, 685 (2002).

[7] D. de Fontaine, M. Asta, R. McCormack, and C. Wolverton, in *New Horizons for Materials*, edited by P. Vincenzini (Techna, Faenza 1995), Vol. 4, pp. 241–246.

[8] J. M. Sanchez and D. de Fontaine, in *Structure and Bonding in Crystals*, edited by M. O'Keeffe and A. Navrotsky (Academic Press, New York, 1981), Vol. 2, 117–132.

[9] S. H. Jhi and J. Ihm, Phys. Rev. B **56**, 13826 (1997).

[10] I.-J. Jung, S. Kang, S.-H. Jhi, and J. Ihm, Acta Mater. **47**, 3241 (1999).

[11] V. T. Em and M. Y. Tashmetov, Phys. Status Solidi B **198**, 571 (1996).

[12] I. Karimov, V. T. Em, V. F. Petrunin, I. S. Latergaus, and V. S. Polishchuk, Neorg. Mater. **12**, 1492 (1976).

[13] V. N. Lipatnikov and A. I. Gusev, JETP Lett. **69**, 669 (1999).

[14] T. Priem, B. Beuneu, C. H. de Novion, A. Finel, and F. Livet, J. Phys. (France) **50**, 2217 (1989).

[15] J. M. Sanchez, F. Ducastelle, and D. Gratias, Physica A **128**, 334 (1984).

[16] G. L. W. Hart, V. Blum, M. J. Walorski, and A. Zunger, Nat. Mater. **4**, 391 (May 2005).

[17] V. Blum, G. L. W. Hart, M. J. Walorski, and A. Zunger, Phys. Rev. B **72**, 165113 (2005).

[18] G. Kresse and J. Furthmüller, Comput. Mater. Sci. **6**, 15 (1996).

[19] G. Kresse and J. Furthmüller, Phys. Rev. B **54**, 11169 (1996).

[20] S. Froyen, Phys. Rev. B **39**, 3168 (1989).

[21] A. van de Walle and G. Ceden, J. Phase Equilib. **23**, 348 (2002).

[22] J. Shao, J. Am. Stat. Assoc. **88**, 486 (1993).

[23] K. Baumann, Trends Analyt. Chem. **22**, 395 (2003).

[24] R. Dronskowski and P. E. Blöchl, J. Phys. Chem. **97**, 8617 (1993).

[25] O. K. Andersen, Phys. Rev. B **12**, 3060 (1975).

[26] O. K. Andersen and O. Jepsen, Phys. Rev. Lett. **53**, 2571 (1984).

[27] G. Kresse and D. Joubert, Phys. Rev. B **59**, 1758 (1999).

[28] P. E. Blöchl, Phys. Rev. B **50**, 17953 (1994).

[29] W. Lengauer, S. Binder, K. Aigner, P. Ettmayer, A. Guillou, J. Debuigne, and G. Groboth, J. Alloys Compd. **217**, 137 (1995).

[30] K. Aigner, W. Lengauer, D. Rafaja, and P. Ettmayer, J. Alloys Compd. **315**, 121 (1994).

[31] V. P. Zhukov, V. A. Gubanov, O. Jepsen, N. E. Christensen, and O. K. Andersen, J. Phys. Chem. Solids **49**, 841 (1988).

[32] A. F. Guillermet and G. Grimvall, Phys. Rev. B **40**, 10582 (1989).

[33] A. R. Guillermet and G. Grimvall, J. Phys. Chem. Solids **53**, 105 (1992).

[34] S.-H. Jhi, J. Ihm, S. G. Louie, and M. L. Cohen, Nature (London) **399**, 132 (1999).

[35] D. D. Fontaine, Solid State Phys. **34**, 73 (1979).

[36] J. M. Cowley, J. Appl. Phys. **21**, 24 (1950).

[37] M. A. Krivoglaz, *Diffuse Scattering of X-Rays and Neutrons by Fluctuations* (Springer, New York, 1996).

[38] L. H. Schwartz and J. B. Cohen, *Diffraction from Materials* (Academic Press, New York, 1977).

[39] Z. W. Lu, D. B. Laks, S.-H. Wei, and A. Zunger, Phys. Rev. B **50**, 6642 (1994).

[40] H. W. Hugosson, P. Korzhavyi, U. Jansson, B. Johansson, and O. Eriksson, Phys. Rev. B **63**, 165116 (2001).

[41] J. O. Kim, J. Achenbach, P. B. Mirkarimi, M. Shinn, and S. A. Barnett, J. Appl. Phys. **72**, 1805 (1992).

[42] R. Chang and L. J. Graham, J. Appl. Phys. **37**, 3778 (1966).

[43] S. P. Dodd, M. Cankurtaran, and B. James, J. Mater. Sci. **38**, 1107 (2003).

[44] The term quasisuperlattice here refers to structures with superlatticelike stacking but where all planes need not be pure. In the present case, quasisuperlattice refers to stacking with all planes either pure or at a 50% concentration [see Fig. 1(b)].